Pierre Auger Project Note: GAP-2000-033

Fluorescence Detector Optical Calibration and Atmospheric Monitoring for the Pierre Auger Experiment

Roger Clay, Bruce Dawson, Russell Pace
University of Adelaide, Adelaide, Australia 5005

Jeffrey Brack, Gertjan Hofman
University of Colorado, Boulder, CO 80309, USA

John A.J. Matthews, Michael Roberts
University of New Mexico, Albuquerque, NM 87131, USA

Brian Fick, Paul Sommers
University of Utah, Salt Lake City, Utah 84112, USA

June 30, 2000 / Revised January 5, 2001

Abstract

A reliable energy scale and energy resolution is central to the mission of the Pierre Auger ultra-high energy cosmic ray experiment. The *hybrid* measurement of a subset of all showers by both the Auger ground array and fluorescence detectors will be used to set the shower energy scale and to measure the shower energy resolution. The uncertainties in the fluorescence energy measurement must therefore be well understood. The major uncertainties come from the calibration of the absolute efficiency of the fluorescence telescopes and from the precision of various atmospheric transmission, air Cherenkov subtraction, light multiple-scattering and cloud corrections to the fluorescence data. These topics are the focus of this paper.

1 Introduction

1.1 Air Shower Measurements by Fluorescence Detectors

Extreme high energy (EHE) cosmic rays produce extensive air showers in the atmosphere. Approximately 50 parts per million of the deposited energy is isotropically re-radiated in fluorescence emission at near-UV wavelengths: 290 $\sim$ 440nm (Bunner 1964, Kakimoto *et al* 1996). Air fluorescence experiments, originally proposed by Greisen (Greisen 1965) and realized successfully first in the Fly's Eye experiment (Bergeson *et al* 1977, Baltrusaitus *et al* 1985), observe the fluorescence light with imaging telescopes. This technique is attractive as it provides both tracking information and the time evolution of the particle cascade. The cascade is measured by observing the shower grow in brightness, reach maximum and then decrease in brightness. The integral of the longitudinal development profile reveals the total electromagnetic shower energy, as the energy is deposited at a rate of $\sim$2.2 MeV/particle/gm/cm^2 (Song *et al* 1999).

The latest generation of EHE experiments: AGASA (Takeda *et al* 1998), High Resolution Fly's Eye (Abu-Zayyad *et al* 1999), and Pierre Auger (Auger 1997), focus on the cosmic ray spectrum near and above the Greisen-Zatsepin-Kuz'min (GZK) cutoff (Greisen 1966, Yoshida 1998). Experimental data (Bird *et al* 1993, Yoshida *et al* 1995, Abu-Zayyad *et al* 1999a) suggest changes in both the power law spectrum and composition at cosmic ray energies just below the GZK cutoff. Theoretical models predict a range of variations in the cosmic ray power law spectrum and composition for cosmic ray energies near and above the GZK cutoff (Bhattacharjee and Sigl 1998, Olinto 2000). To be sensitive to energy dependent details, experiments must calibrate their (absolute) energy scale and control (non-Gaussian) energy measurement errors. In Auger the (absolute) energy scale of the ground array will be determined using the reconstructed fluorescence detector energies from *hybrid* events; *i.e.* events where the ground array and the air fluorescence detectors observe the same shower(s). Hybrid showers, and *stereo* fluorescence showers observed by more than one fluorescence detector, provide a sample of data with two (or more) independent energy measurements. These can be compared (Bird *et al* 1994) to monitor experimentally the shower energy resolution.

Thus the Auger energy measurements depend on the precision of the air fluorescence measurements. The precision of the air fluorescence measurements in turn depends on several uncertainties. Two of these, the fraction of detectable shower energy (Song *et al* 1999) and the fraction of electromagnetic energy loss (in air) that appears as fluorescence light (Kakimoto *et al* 1996), contribute $\sim$ 5% and $\sim$ 10% systematic uncertainties respectively to the fluorescence energy measurement. The other major uncertainties in the fluorescence energy measurements come from the calibration of the absolute efficiency of the fluorescence telescopes and from the precision of various atmospheric transmission, air Cherenkov subtraction, light multiple-scattering and cloud

corrections to the fluorescence data. These topics are the focus of this paper.

The atmospheric corrections can be understood by noting that the atmosphere has two important roles in Auger: it is the showering medium for the primary cosmic ray and, for the Auger air fluorescence detectors, it is also an essential part of the readout system. Thus like any component of a readout system, the atmosphere must be calibrated, the calibration monitored with time and the atmospheric calibrations input to the analysis of the fluorescence data.

The plan for the paper is as follows. In Sect. 2 we review how the atmosphere influences air fluorescence measurements. Consequently corrections must be applied to the fluorescence data. The experimental determination of these corrections defines the atmospheric monitoring requirements for the experiment. In Sect. 2.1 the Auger monitoring for atmospheric transmission, air Cherenkov subtraction, and light multiple-scattering corrections are described. In Sect. 2.2 cloud monitoring for Auger is presented. In Sect. 3 we briefly summarize the components that make-up the photon detection efficiency of the fluorescence telescopes and then present the Auger plan to do an inclusive (or end-to-end) calibration, *i.e.* UV-photon signal to ADC value, for the Auger fluorescence telescopes. Finally Sect. 4 provides a summary.

2 Atmospheric Monitoring for Auger Fluorescence Detectors

The air fluorescence measurements are influenced by the scattering and absorption of light in the atmosphere. To minimize these effects, fluorescence experiments are located in dry desert areas with typically excellent visibility. Nevertheless some scattering and absorption does occur. Sect. 2.1 discusses the atmospheric characterization and corrections for the Auger fluorescence data.

Clouds near the shower and/or between the shower and the fluorescence telescope(s) significantly alter the fluorescence signal. Sect. 2.2 discusses the detection and tracking of clouds in Auger.

2.1 Atmospheric Characterization and Corrections in Auger

Light scattering (dominant term) and absorption in the atmosphere changes the transmission efficiency of light from the extensive air shower to the fluorescence telescopes from unity. The observed light intensity, I, can be related to the light intensity of the (isotropic) source, I_0, as follows:

$$I \;=\; I_0 \cdot T^m \cdot T^a \cdot (1. \;+\; H.O.) \cdot \frac{d\Omega}{4\pi}$$

where T^m and T^a are the transmission factors for the *molecular* and *aerosol* scattering parts of the atmosphere, $H.O.$ is a higher order correction (also known as multiple-scattering or aureole) and $d\Omega$ is the solid angle subtended by the observing telescope.

To obtain the source light intensity, I_0, from the measured intensity, I, each of the (correction) factors in the expression above must be known. Uncertainties in the source light intensity will arise from uncertainties in each of the (correction) factors. As the shower energy is proportional to the fluorescence light signal, the uncertainty in the reconstructed shower energy, ΔE, from *e.g.* a transmission uncertainty, ΔT, is given by:

$$\frac{\Delta E}{E} \quad = \quad \frac{\Delta I_0}{I_0} \quad = \quad \frac{\Delta T}{T}$$

Thus a *e.g.* 10% uncertainty in transmission correction results in a 10% uncertainty in shower energy.

Two different light scattering sources dominate in the near-UV wavelengths relevant to the Auger experiment. These are Rayleigh scattering, which describes the scattering of light in a pure or molecular atmosphere, and Mie scattering, which describes the scattering of light on much larger scattering centers in the atmosphere called aerosols. In practice the Rayleigh scattering related corrections, while large, can be made with precision. In contrast the corrections related to Mie scattering, while typically less than the Rayleigh corrections, are *a priori* unknown. Thus most of the atmospheric monitoring is focused on the Mie/aerosol component.

In addition to the transmission corrections, which depend on the total Rayleigh and Mie scattering cross sections and integral density of scatterers, the air Cherenkov (Cassiday *et al* 1990) and multiple scattering ($H.O.$) corrections require knowledge of the differential scattering cross sections and local density of scatterers. The measurement and monitoring of the Mie aerosol phase function (normalized differential scattering cross section) is presented in Sect. 2.1.3 below.

It is instructive to review the form of the Rayleigh transmission correction. As a consequence of Rayleigh scattering, the apparent intensity from a source decreases exponentially with travel distance through the atmosphere. The multiplicative *molecular transmission* is given by:

$$T^m \quad \equiv \quad T^m(z,\alpha,\lambda) \quad = \quad e^{-\int_0^z \frac{\rho^m(z)dz}{\Lambda^m(\lambda)} \cdot \frac{1}{sin(\alpha)}}$$

where z is the vertical height of the light source above the fluorescence telescope and $z = 0$ is defined as the altitude of the fluorescence telescope(s). $\rho^m(z)$ is the air density versus height and α is the elevation angle of the light path. This geometry is shown schematically in Fig. 1. Finally $\Lambda^m(\lambda) = 2974 \cdot (\frac{\lambda}{400nm})^4$ gm/cm^2 is the Rayleigh extinction length as a function of wavelength, λ (Flowers *et al* 1969). At an Auger site

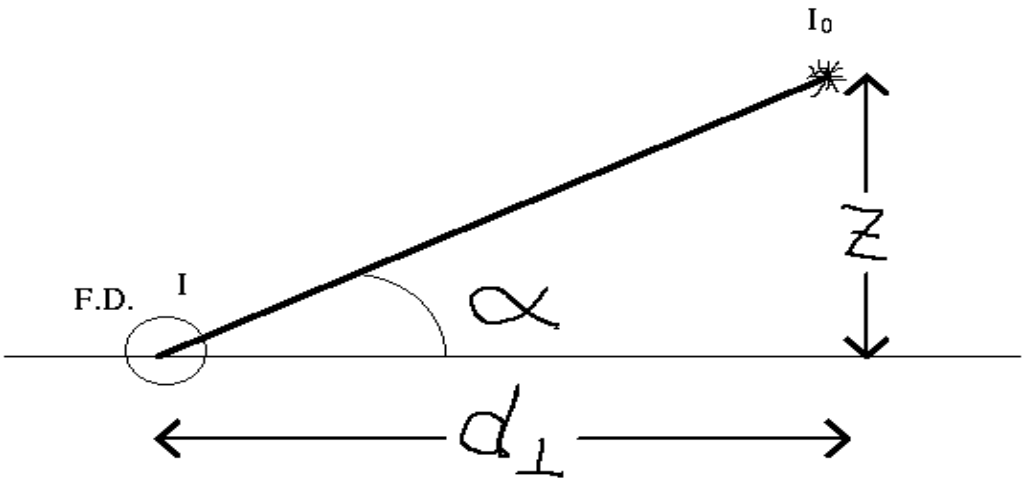

Fig. 1: Sketch of light path from source of intensity, I_0, to the observed intensity, I, at the fluorescence detector. The source is in the field of view of the photo-tube viewing at an angle α to the horizontal. The source height, z, and horizontal distance, $d_\perp$, are simply related by $tan(\alpha)$.

altitude of $\sim$ 1500m, this corresponds to $\Lambda^m(\lambda) \sim 18.4$ km at 360nm (approximate middle of Auger wavelength acceptance).

The molecular transmission, T^m, factors into a height-wavelength dependent part, called the *molecular optical depth*, $\tau^m(z,\lambda) = \int_0^z \frac{\rho(z)dz}{\Lambda^m(\lambda)}$, and into a slant factor, $\frac{1}{sin(\alpha)}$, where $\frac{z}{sin(\alpha)}$ is the full length of the light path. This factorization reflects the 1-dimensional nature of the molecular atmosphere. The further factorization of $\tau^m(z,\lambda)$ into a height dependent part, $\int_0^z \rho(z)dz$, and into a wavelength dependent part, $\frac{1}{\Lambda^m(\lambda)}$, reflects the fact that the composition of the molecular atmosphere is independent of height.

To achieve $\frac{\Delta T^m}{T^m} < 2 \sim 3\%$ it is sufficient to monitor the temperature, $T(0)$, and pressure, $P(0)$, at the fluorescence telescopes. The adiabatic component of the U.S. Standard Atmosphere model (CRC 1991, Martin and Matthews 1999) then provides a good model for $\rho^m(z)$ for altitudes (to $\sim$ 10km) above the telescopes:

$$T(z) = T(0) - 6.5°K \cdot z(km)$$

$$P(z) = P(0) \cdot (T(z)/T(0))^{5.255877}$$

$$\rho(z) = 0.3483677 \cdot (P(z)/T(z))$$

Mie scattering of light on aerosols results in an additional exponential decrease of the light intensity with distance from the light source. The 1-dimensional Rayleigh atmosphere provides a guide to model the aerosol multiplicative *aerosol transmission*:

$$T^a \equiv T^a(z,\alpha,\lambda) = e^{-\int_0^z \frac{\tilde{\rho}^a(z)dz}{\Lambda^a(\lambda)} \cdot \frac{1}{sin(\alpha)}}$$

where $\tilde{\rho}^a(z) = \rho^a(z)/\rho^a(0)$ is the normalized density of aerosols *versus* altitude. It is typical, but not essential, to parameterize $\tilde{\rho}^a(z)$ as $\tilde{\rho}^a(z) = e^{-z/h_a}$. $\Lambda^a(\lambda)$ is the aerosol extinction length (*e.g.* in meters) as a function of wavelength measured at the height of the fluorescence telescopes. Representative desert values are: $h_a \sim 1.2$km and $\Lambda^a(\lambda = 360nm) \sim 20$km (Sokolsky 1996). As with the molecular transmission, the aerosol transmission can be re-expressed in terms of the *aerosol optical depth*, $\tau^a(z,\lambda) = \int_0^z \frac{\tilde{\rho}^a(z)dz}{\Lambda^a(\lambda)}$ and slant factor.

The above model for aerosols copies the structure of the molecular atmosphere. Thus implicit in this aerosol model are two assumptions which while true for the molecular atmosphere may not be true for the aerosols. First that the aerosol vertical variations are much more important than the horizontal variations; *i.e.* we use a 1-dimensional model. A 1-dimensional model is not un-typical of the night time atmosphere in large, desert valleys at locations well away from the valley walls (Seinfeld and Pandis 1998). Second the vertical profile of the aerosols is the same at all wavelengths in our wavelength interval of interest, $300nm \sim \lambda \sim 400nm$ set by UV filters in the fluorescence telescope (Wilkinson 1998). Thus we assume that to first order the wavelength dependence is only in the extinction length, $\Lambda^a(\lambda)$. In this approximation if $T^a(z,\alpha,\lambda)$ is known at 355nm, the wavelength of frequency tripled YAG lasers used to monitor the atmosphere, then:

$$T^a(z,\alpha,\lambda) = (T^a(z,\alpha,355nm))^{\frac{\Lambda^a(355nm)}{\Lambda^a(\lambda)}} = (T^a(z,\alpha,355nm))^{R(\lambda)}$$

The exponent, $R(\lambda)$, is expected to vary with time and will be routinely monitored. Typical values of $R(\lambda)$ for a desert atmosphere are predicted in the range: $0.91 \sim 1.14$ (Longtin *et al* 1988).

Representative examples of molecular (Rayleigh) and aerosol (Mie) transmission factors are shown in Fig. 2a and b. The transmission factors depend on the viewing angle of the fluorescence telescope, α, and the horizontal distance of the light source from the fluorescence detector site (see Fig. 1). The molecular and aerosol transmission curves look different for two reasons: the horizontal extinction lengths are (slightly) different, $\Lambda^m \sim 18.4$km *versus* $\Lambda^a = 20$km, and the vertical scale heights are very different, $h_m \sim 7.5$km *versus* $h_a = 1.2$km. While any given air shower may be viewed over a wide range of viewing angles the energy measurement is most sensitive in the direction of shower maximum. In this case the $\alpha \approx 10^\circ$ is rather typical.

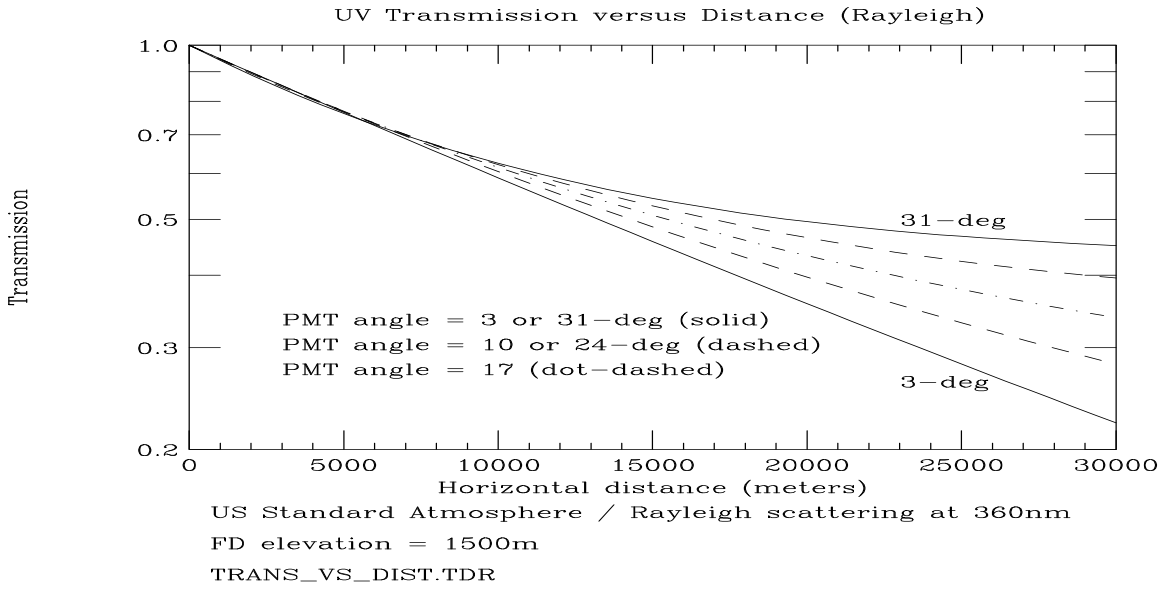

Fig. 2a: Transmission factor, T^m, for Rayleigh scattering on the molecular atmosphere. Curves are shown for Auger fluorescence telescope viewing angles from $3^\circ \sim 31^\circ$ to the horizon.

The aerosol transmission correction factor will be monitored using the 1-dimensional model described above. In this model two quantities are to be determined: the horizontal extinction length, $\Lambda^a(\lambda)$, at the altitude of the fluorescence detector sites and the integral to height, z, of the vertical profile of the aerosols, $\int_0^z \tilde{\rho}^a(z)dz$. This will be done using dedicated instruments. The horizontal extinction length will be monitored using mercury vapor light sources at (two) large distances from CCD-based photometers. Interference filters allow individual mercury lines to be monitored. This is summarized in Sect 2.1.1. The integral to height, z, of the vertical profile of the aerosols will be monitored using backscattered LIDARs. This is summarized in Sect 2.1.2. LIDARs will be operated at several of the Auger fluorescence sites; the fluorescence sites are separated by $\sim$ 25km. Comparison of the results from the different sites, and from monitoring in different directions at each site, will monitor deviations from the 1-dimensional aerosol model.

2.1.1 Horizontal extinction length monitor

The goal of the horizontal extinction length measurement is to determine the combined Rayleigh and Mie horizontal extinction length, $\Lambda(\lambda)$:

$$\frac{1}{\Lambda(\lambda)} = \frac{1}{\Lambda^m(\lambda)} + \frac{1}{\Lambda^a(\lambda)} \quad (1)$$

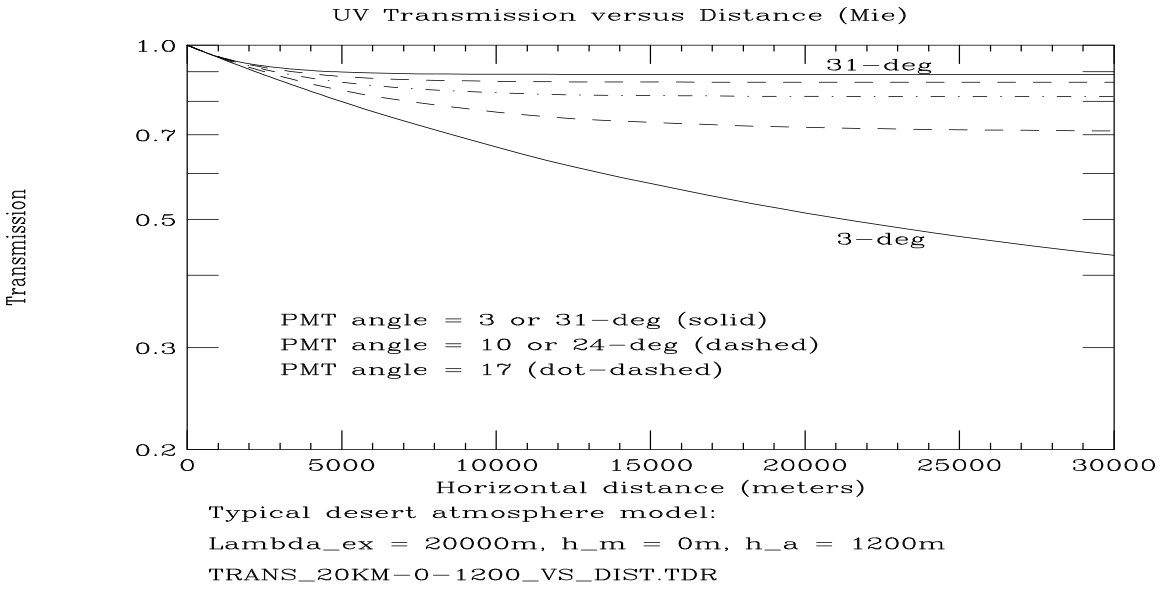

Fig. 2b: Transmission factor, T^a, for Mie scattering on aerosols in the atmosphere. The aerosols are described by a horizontal extinction length, $\Lambda^a(360nm) = 20$km and an exponential scale height, $h_a = 1200$m. Curves are shown for Auger fluorescence telescope viewing angles from $3° \sim 31°$ to the horizon.

at several wavelengths, λ, in and near the wavelength acceptance of the fluorescence detectors. The measurement are made at typically one hour time intervals during nights of fluorescence data taking. For Auger two such measurements will be made. As these will use independent instrumentation and will monitor very different light paths across the site, they will provide information on site and instrument related systematic uncertainties in the horizontal extinction length.

The measurement is made using a stable light source viewed by a stable photometer. The photometer signal, $S(r, \lambda)$, at a horizontal distance, r, from a point source of intensity, I_0, is given by:

$$S(r,\lambda) \quad \propto \quad \frac{I_0}{r^2} \cdot e^{-\frac{r}{\Lambda(\lambda)}}$$

The standard procedure (Optec 2000) is to measure the intensity at two distances from the source: a *near* measurement $\sim$ 1km from the source and a *far* measurement $\sim$ 50km from the source. The measurements are made using one photometer. The photometer is normally positioned at the *far* location. The near measurement is made a few times each year. For these measurements the photometer is physically moved to a location *near* the light source. At this location the exponential attenuation term

is nearly one. Thus the *near* measurement in effect measures the product of the light intensity, I_0, and photometer detection efficiency. The ratio of the *near* intensity to *far* intensity provides a sensitive and simple measurement of the extinction length:

$$\Lambda(\lambda) \quad = \quad \frac{(r_{far} - r_{near})}{ln(\ \frac{S^{obs}_{near}(\lambda)}{S^{obs}_{far}(\lambda)}\ \cdot\ (\frac{r_{near}}{r_{far}})^2\ )}$$

Using Eqn. 1, the aerosol/Mie extinction length, Λ^a, can then be determined by subtracting the molecular/Rayleigh extinction length, Λ^m, calculated with the local atmospheric temperature and pressure as summarized in Sect 2.1 above.

The new features unique to Auger are to extend the Optec (Optec 2000) technique to near UV wavelengths and to make the measurements at several different wavelengths. The details are provided in Appendix 1.

2.1.2 Integral vertical profile monitor

The (integral) vertical profile of the aerosols in the atmosphere will be monitored using steerable, backscattered LIDARs. Each backscattered LIDAR consists of a pulsed laser beam and a receiver telescope composed of a mirror and a gated, high-speed photon detector. The receiver is located at the same place as the laser and is aligned to point in the laser beam direction. The receiver measures the back-scattered photons as a function of time or equivalently the intensity of the photons *versus* distance to the point the light back-scattered. The observed intensity at an angle, α to the horizontal, is given by,

$$I(z,\alpha) \quad = \quad I_0 \cdot T_{out} \cdot T_{back} \cdot \sum_j\ \frac{1}{\Lambda^j(z)} \frac{1}{\sigma^j} (\frac{d\sigma^j}{d\Omega})_{180^\circ}\ \cdot \Delta s \cdot \Delta\Omega$$

where I_0 is the out-going LIDAR beam intensity, T_{out} and T_{back} are the transmission factors for the (out-going) light beam and for the scattered (back-coming) light respectively, $\Lambda(z)$ are the attenuation lengths at height z, $\Delta s = c\Delta t/2$ is the length of the scattering region (set by the LIDAR time bins), $\Delta\Omega$ is the solid angle subtended by the LIDAR mirror, and $\frac{1}{\sigma^j}(\frac{d\sigma^j}{d\Omega})$ are the Rayleigh and Mie *phase functions* for $j \equiv m, a$ respectively. In the absence of *H.O.* corrections (which are minimized using narrow field of view LIDAR receivers), the transmission for the out-going light, T_{out}, and the back-coming light, T_{back}, are equal. By taking ratios of backscattered LIDAR measurements, $I(z,\alpha)$, from the same altitude, z, but at different angles, α, the phase functions and attenuation lengths (which are unknown in the case of aerosol scattering) cancel and the sum of Rayleigh (molecular) and Mie (aerosol) optical depths is obtained. The details are provided in Appendix 2. The aerosol optical depth is obtained by subtracting the relatively well known molecular optical depth. Finally the integral to height,

z, of the aerosol vertical profile is then obtained from the (measured) aerosol optical depth: $\int_0^z \tilde{\rho}^a(z)dz \;=\; \tau^a(z,\lambda)\cdot\Lambda(\lambda)$.

In the constant composition, 1-dimension model for aerosols the integral to height, z, of the aerosol vertical profile need not be measured in the wavelength acceptance of the fluorescence telescopes, $300 \sim 400$nm. Thus it may be sufficient to measure the vertical profile of aerosols at somewhat longer wavelengths (*e.g.* 532nm) where the fluorescence detectors are insensitive. At these wavelengths a LIDAR can be co-sited at a fluorescence site with minimal impact on the operation of the fluorescence telescopes. This possibility is presently under study by the Auger collaboration.

2.1.3 Aerosol phase function monitor

The observed light from an extensive air shower includes both the air fluorescence signal plus some of the Cherenkov light that is part of the air shower. The air shower Cherenkov light is mostly in a few degree cone centered on the air shower axis (Baltrusaitis *et al* 1987). Through scattering of the Cherenkov light in the air, some of the Cherenkov light appears as a background in the fluorescence data. This background is estimated and subtracted as part of the analysis of each fluorescence event (Cassiday *et al* 1990)). Furthermore air showers with shower axes pointing within $\sim 20^\circ$ of the direction to a fluorescence site are excluded from analysis to minimize this correction (Cassiday *et al* 1990)). To estimate the fraction of Cherenkov light scattered on aerosols we need the aerosol attenuation length, $\Lambda^a(z) \;=\; \Lambda^a(0)/\tilde{\rho}^a(z)$ (at height z above the fluorescence detectors), and the aerosol phase function (normalized aerosol differential scattering cross section), $\frac{1}{\sigma^a}(\frac{d\sigma^a}{d\Omega})$. For the Cherenkov light correction, the aerosol phase function must be known for scattering angles to within $\sim 10^\circ$ of the initial light direction.

The observed light from an extensive air shower will also include a contribution of multiple scattered light. This will be true for the air fluorescence signal and for the Cherenkov background light. Initial estimates of the effect (Zhang 2000), show that the fractional increase in the observed light intensity is greatest for the most distant showers. The size of the correction can be reduced by restricting the time interval (for each photo-tube contributing to the reconstructed shower) and the angular acceptance (transverse to the shower axis) of the data used in shower reconstruction. Conversely light (in a given photo-tube) observed earlier or later than expected provides a monitor of the intensity of the multiple scattered light. Similarly light observed in photo-tubes removed from the shower axis are also a monitor of the intensity of the multiple scattered light. As Auger telescopes have good optics (*i.e.* almost no stray light) and digitize the fluorescence light in 100ns time intervals rather detailed information on the multiple scattered light is expected (Roberts 2000).

The correction for multiple scattered light in the fluorescence signal is made using Monte Carlo or iterative methods. Both techniques require knowledge of the aerosol

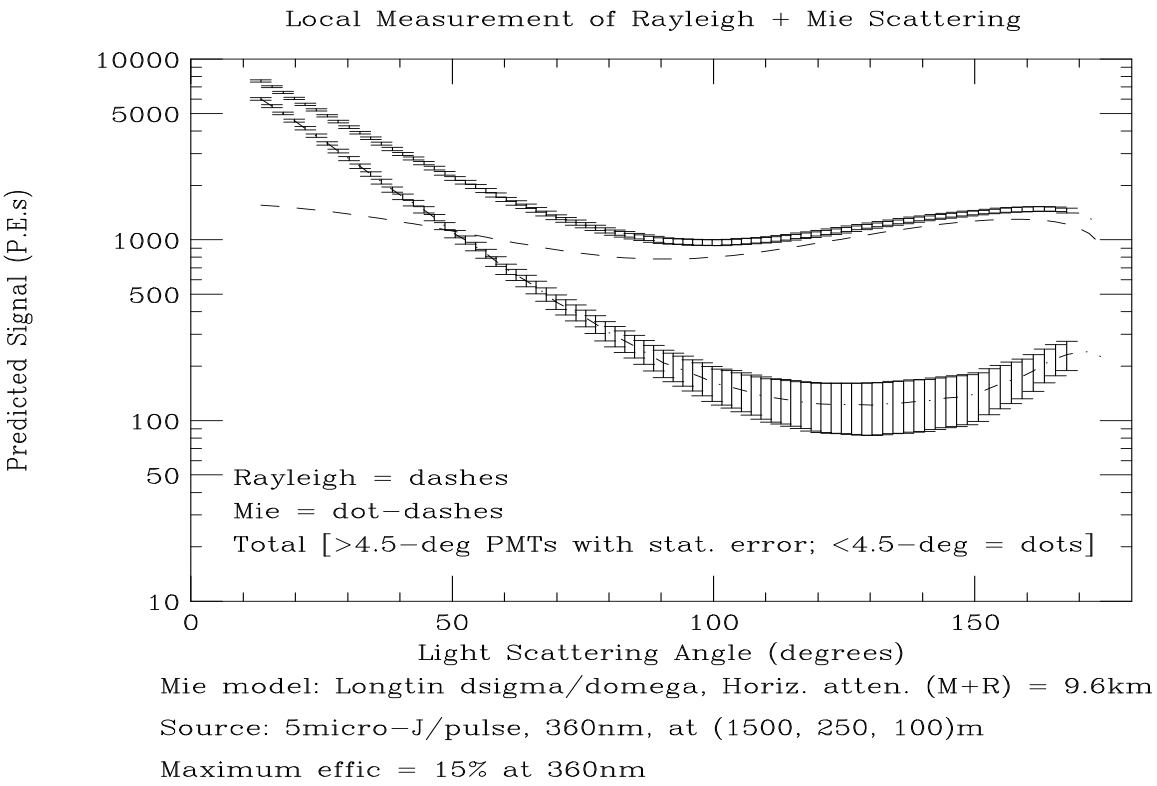

Fig. 3: Simulated signal in an Auger fluorescence detector from a pulsed 360nm light beam passing 100m above and 250m horizontally from the fluorescence site. The light source is positioned 1.5km from the fluorescence site. The Rayleigh scattering is based on a US Standard Model atmosphere. The Mie scattering assumes a 20km attenuation length and a 1.2km (vertical) scale height. The top curve is the combined Rayleigh plus Mie signal. The bottom curve has the Rayleigh contribution subtracted. The error bars include photo-electron statistical errors and night sky noise.

phase function at all scattering angels. In practice it is most important to know the Mie phase function at more forward scattering angles where Mie dominates Rayleigh scattering.

In the constant composition, 1-dimensional model for aerosols it is sufficient to measure the aerosol phase function at the altitude of the fluorescence detectors. The measurement can then be made using a near-horizontal, pulsed light beam directed across the field of view of one of the fluorescence sites (Tessier *et al* 1999). As each fluorescence site views $\sim 180^\circ$ in azimuth, even a fixed direction light beam will allow the aerosol phase function to be measured over most of the range of scattering angles. As an example, Fig. 3 shows the simulated signal (observed in the Auger fluorescence detectors) from a 5μJ/pulse, 360nm light source located 1.5km from the fluorescence

site (with the light beam directed so as to pass within 250m horizontally and 100m vertically from the fluorescence detectors). As the light paths, from this light source to the fluorescence detectors, are much less than the total atmospheric extinction length the transmission and multiple scattering corrections are small.

2.1.4 **Overall consistency** *cross check*

To check the constant composition, 1-dimension aerosol model assumed by our analysis, at least one steerable, 355nm laser should be placed near the boundary of the Auger site and 15 $\sim$ 20km from the nearest fluorescence detector site. The *side* scattered light from this laser will be observed by one or more of the the fluorescence detectors. A comparison of the predicted *versus* observed signal (as a function of time) provides the essential cross check of the aerosol model and the ingredients of the model: the horizontal attenuation length, the vertical profile of aerosols and the aerosol phase function.

2.2 Cloud Detection and Monitoring in Auger

The possible presence of cloud while fluorescence observations are in progress is a cause for concern. The level of cloud cover is a factor in determining the collecting area available to the fluorescence detectors. Unlike smaller cosmic ray experiments, it is quite possible that parts of the atmospheric fiducial volume of the Pierre Auger Observatory will be usable while other parts are not. Additionally, the presence of small, or broken regions of cloud in an otherwise clear sky can lead to uncertainty in the interpretation of shower profiles. If a profile were to be recorded with significant (local) fluctuations in intensity, it may not be clear whether that was due to shower physics or to cloud obscuration and/or to thin cloud scattering of the shower Cherenkov light.

Daytime cloud is readily detectable against sky background because its droplet content scatters visible sunlight differently to atmospheric gas, both in its wavelength dependence and its total cross section. Also, the background atmosphere is rather uniform in intensity due to the high scattering cross section of blue sunlight. At night, in the absence of sunlight, clouds are not visible by optical scattering and there is a very non-uniform sky background, against which an observer might try to see the presence of clouds by their background obscuration. Nonetheless, the recording of cloud conditions by the casual observations of non dark-adapted observers is a common default technique. The Pierre Auger Project recognized that systematic cloud monitoring in an objective manner was required. This has proved possible using infra-red observations at wavelengths of about 10μm.

Clouds are in a form of thermal equilibrium with their surrounding atmospheric

gas. This is at a temperature somewhat below that of the ground and they radiate rather like a black body at wavelengths appropriate to that temperature. Wien's law tells us that those wavelengths are of the order of 10μm and, at those wavelengths, the clear sky is much less intense. It is then possible to detect clouds by their strong infra-red emission, against a much weaker clear sky background. From a practical aspect, all that is required in order to detect clouds is to have a detector sensitive to the appropriate range of wavelengths and to monitor its output while it points at a particular part of the sky. This is now straightforward and economical. Such a detector has been described by Clay *et al* (1998) based on a Heimann TPS 534 infra-red sensor element.

The efficient detection of clouds at large distances is more complex than the mere observation of clouds above an observer. The distances are greater, clouds of a given dimension are smaller on an angular scale, and, more seriously, the atmosphere itself becomes brighter towards the horizon where one inevitably wishes to view distant clouds. Experience with the High Resolution Fly's Eye is that a temperature resolution at least as good as 1K is required to efficiently locate cloud at low altitudes.

A key paper in the field was by Sloan, Shaw and Williams (1955). They showed that infra-red cloud detection was straightforward but that the clear sky emissivity, and hence the brightness close to the horizon, was strongly dependent on atmospheric humidity. Their data also indicated that the humidity dependence was not limited to conventional molecular bands such as at 6.3μm, but was spread over the whole spectrum. An improvement in signal to noise is possible by avoiding known atmospheric emission bands, but a vapor pressure (or integrated water vapor content) dependence remains through the continuum emission. The resulting clear sky emissivity has been discussed by Prata (1996).

A particular problem, not previously discussed, is the need of the Pierre Auger cloud system to both locate cloud above a point on the ground, and to determine its altitude. This may be possible by triangulation but other height information would be very helpful. Buckley *et al* (1999) have discussed the use of infra-red radiometers for cloud detection in an astrophysical context and have highlighted a number of important issues, including the possible dependence of the infra-red signal on cloud height. We have compared ceilometer data and cloud temperature measurements, made with a narrow angle infra-red radiometer, to examine this possibility. Our data are not as optimistic as those previously reported. There is a temperature/altitude dependence but it is not clear cut. This may be due to distortions of the temperature lapse rate below the cloud or the uncertain emissivity properties of cloud over the whole wavelength range available to the radiometer.

2.2.1 Sensitivity of an Infra-red Detector

The lens system of an infra-red detector (which may consist of a filter, focusing lens, infra-red transparent protective covers or any combination of these) facilitates heat exchange between the source and the detecting element. Any significant temperature difference between these two will result in a measurable temperature change in the detecting element. However, the detecting element is sensitive to more than just the flux from the source. Any objects at or near ambient temperature (including the enclosure around the detecting element and the lens system) will absorb, emit and reflect infra-red radiation in the bandpass of the sensor. These infra-red emissions are indistinguishable from the source flux, and any variation in them will introduce changes in the output signal. This ambient flux contribution is dependent on the geometry of the sensor system, the infra-red properties of the various materials (ie emissivity, reflectivity and transmissivity) and the object temperatures. Choppers and similar occulting devices are often used to determine any resulting offsets.

For a thermopile (eg as used in the Heimann TPS 534 sensor) the output voltage is approximately proportional to the temperature difference between the detecting element and a reference element held at ambient temperature. As the ambient temperature changes so does the reference zero voltage point, requiring compensation of the output signal.

Ultimately the minimum detectable flux is dependent on the noise in the signal which arises in two main ways 1) the temperature fluctuations in the detecting element due to radiative or conductive heat exchange with the background and 2) Johnson noise, both of which exhibit temperature dependencies.

A blackbody, by definition, is a perfect absorber and perfect emitter at all wavelengths. However for real objects some fraction of the incoming radiation is reflected r, some absorbed a and (possibly) some transmitted t, such that $a+r+t=1$. A fundamental principle is that for equilibrium conditions the absorptivity of an object equals its emissivity. In general that emissivity (defined as $\varepsilon = flux/\sigma T^4$) is affected by the composition of the body, its temperature, the extent of surface roughness and angle of observation with the emitting surface. For transmissivity, the thickness and shape of the body are also relevant.

For any radiometer consisting of a sensor and lens system the following relationship can be derived (eg after Harrison 1960) which characterizes the various parameters that contribute to the flux incident on the detecting element.

$$W_{net} = t_l \varepsilon_d A_d \sin^2 \theta_d \sigma (f_s \varepsilon_s T_s^4 - f_a \varepsilon_a T_a^4)$$

where W_{net} is the net flux in excess of that received at $T_s = T_a$. The subscripts 's', 'l', 'd' and 'a' refer respectively to the *source* as acquired through the lens, the *lens* system, the *detecting* element and the *ambient* environment. t_l is the transmissivity of the lens system, A_d is the area of the detecting element, θ_d is the half angle of the

field of view, ε is the average emissivity, f is the fraction of the total flux emitted in the bandpass of the sensor, T is the temperature and σ is the Stefan-Boltzmann constant. The output voltage, which may be positive or negative depending on the source and reference temperatures, is derived using $V = GRW$ where G is the gain of the supporting electronics and R, which has a small temperature dependency, is the specified sensitivity of the detector (in volts/watt).

The flux expression for a sky detector can be simplified by using an empirical relationship for the sky emissivity (eg Idso 1981, Prata 1996).

$$W_{net} = t_l A_d \sin^2\theta \sigma T_a^4 (\varepsilon_{sky} - f_a \varepsilon_a)$$

where it has been assumed that $\varepsilon_d \simeq 1$ and ε_{sky} ($\equiv f_s \varepsilon_s$) is some function of the ambient temperature T_a, zenith viewing angle and surface water vapor pressure.

The flux contribution from a cloud is greater than that from a colder sky and will increase the temperature of the detecting element. However the precise amount will be dependent on the emissivity of the cloud. This can vary widely ($\sim 0 \rightarrow 1$) depending on several factors including the cloud type, thickness and composition. For thick water clouds, the assumption of an emissivity close to 1 would not be unreasonable. However the emissivity of higher altitude clouds containing ice can be more difficult to predict (Paltridge *et al* 1981). The increased flux contribution to the clear sky signal from a cloud with emissivity ε_c at temperature T_c and angular size θ_c ($\leq \theta_d$) can be estimated using,

$$W_c = t_{sky} t_l A_d \sin^2\theta_c f_c \varepsilon_c \sigma T_c^4$$

where the transmissivity of the air beneath the cloud $t_{sky} \simeq 1 - \varepsilon_{sky}$.

2.2.2 Infra-red Sky Imaging

In order to make the best use of cloud detectors within the Pierre Auger Project, it is both necessary to know that clouds exist and to be able to locate them, preferably in altitude as well as in plan. We have carefully examined the possibility of using vertical viewing single pixel radiometers at all (or a subset) of the ground array detectors. This appears to work well and gives the plan distribution of the clouds. The altitude determination is then difficult if the cloud temperature as a function of altitude is not known with certainty. We have then considered scanning detectors based on our single pixels. These are economical, and can be reliable, but have a pixel field of view of 3° (determined by the finite size of the detecting element and the need to scan in a short time) which still results in limited altitude resolution over the large distances necessary for the huge Auger array. We are currently examining the possible use of (much more expensive) commercial infra-red imaging cameras to be sited, and scanned, at the four fluorescence sites. Image processing would determine the existence and angular location

of clouds and triangulation between detectors would determine the cloud position in three dimensions.

3 End-to-End Optical Calibration for Auger Fluorescence Detectors

The raw data read out from the Auger fluorescence detector will be in the form of flash ADC values corresponding to the intensities seen by the photomultiplier tubes triggered during a given event. An absolute calibration of the telescope must relate these ADC values to the flux of photons incident on the detector, including effects of the UV filter at the telescope aperture, mirror, mercedes cones, PMT response, front end electronics, cables, the ADC, etc. While in principle each of these could be measured separately, the Auger experiment will use an *end-to-end* technique measuring the combined effect. This calibration, along with the atmospheric corrections described above, will complete the chain connecting the ADC values to the number of photons produced in the shower.

The end-to-end absolute calibration system is based on a portable uniform light source which mounts on the external wall of the fluorescence detector building and illuminates the entire entrance aperture of the telescope being calibrated. Telescopes will be calibrated one at a time. The source consists of a pulsed xenon flasher that illuminates a diffusely reflecting hemispherical shell. Photomultipliers mounted at the entrance aperture will monitor the intensity of each pulse. Each pulse will uniformly illuminate the telescope entrance aperture and trigger all the PMTs in the telescope camera.

The success of such a system depends on the ability to calibrate and monitor the intensity and uniformity of the light source. To this end an optics laboratory is being constructed to establish the absolute calibration of the source and the monitoring PMTs. The basic laboratory components will include a D_2 UV light source, diffraction grating monochromator, beam splitter, a NIST calibrated UV Silicon (Si) detector, and a UV sensitive CCD camera.

Several relative measurements will be made in the laboratory. The relative uniformity of the source intensity over the entrance aperture, and the relative intensity as a function of angle, will be measured using a CCD camera with established pixel gains and pedestals. With the camera mounted at varying angles relative to the source surface and appropriately focused, the intensity at many thousands of points on the surface can be measured with a single exposure.

The absolute calibrations will be made using techniques paralleling those used by Larson (Larson *et al* 1998), where the detector to be calibrated is compared to a known standard detector under identical conditions. The detectors to be calibrated are the

diffuse surface monitor PMTs. The calibration standard for the Auger laboratory will be a NIST–calibrated UV Si detector. The monochromator will scan UV wavelengths between 300 and 400 nm using the D_2 source as input. The beam splitter sits at the monochromator output. With Si reference standard and PMT monitor detectors viewing the two beams from the splitter, detector outputs as a function of wavelength can be compared. A ratio of the outputs at a given wavelength gives the calibration of the detector relative to the standard at that wavelength.

The uncertainties in the overall calibration are expected to be dominated by uncertainties in the stability of the monitoring PMTs in the field, in the spacial and angular uniformity of the light source, and in the cumulative uncertainties of calibrating the monitoring PMTs relative to the UV Si calibration detector. Each of these contributions to the overall uncertainty is expected to be less than 5%, giving a total absolute uncertainty on the order of 8% or less.

The estimated uncertainty in the calibration of the monitoring PMTs will include the uncertainty in the UV Si detector calibration, provided by NIST. For these detectors, NIST lists calibration uncertainties varying from 2.06% at 300 nm to 1.46% at 400 nm.

4 Summary

The major uncertainties in the fluorescence detector measurement of the fluorescence light produced by extensive air showers were reviewed and the planned fluorescence detector calibration and atmospheric monitoring procedures for the Auger southern observatory were summarized. The Auger procedures build on the experience of the High Resolution Fly's Eye experiment and take advantage of several unique features of the Auger experiment including Schmidt fluorescence detector optics and the presence of the Auger ground array.

Acknowledgements

The development of atmospheric monitoring procedures and techniques for the Auger experiment has build on and profitted from the pioneering work of the High Resolution Fly's Eye (HiRes) collaboration. The Auger procedures have been matured in cooperation with HiRes and Telescope Array collaborations.

References

Abu-Zayyad T., *et al* 1999 26^{th} Inter. Cosmic Ray Conf., Salt Lake City, **3**, 264

————————- 1999a Phys. Rev. Lett. **84**, 4276

Auger, 1997 Pierre Auger Project Design Report, http://www.auger.org/admin/DesignReport/index.html

Baltrusaitis R. M., *et al* 1985 Nucl. Instrum. Methods **A240**, 410

————————- 1987 J. Phys. G: Nucl. Phys. **13**, 115

Bergeson H. E., *et al* 1977 Phys. Rev. Lett. **39**, 847

Bhattacharjee P. and Sigl G. 1999 astro-ph/9811011 V2, to appear in Phys. Reports

Buckley D. J., *et al* 1999 *Experimental Astronomy* **9** 237

Bird D. J., *et al* 1993 Phys. Rev. Lett. **21**, 3401

———————— 1994 Astrophys. J. **424**, 491

Bunner A. N. 1967 Ph.D. Thesis, Cornell University, Ithaca, N.Y.

Clay R. W., *et al* 1998 *Pub. Astron. Soc. Aust.* **15** 334

Cassiday, G. L., *et al* 1990 Astrophys. J. **356**, 669

CRC 1991 Handook of Chemistry and Physics, 72^{nd} Ed., 14-11

Flowers E. C., McCormick R. A. and Kurfis J. 1969 J. Appl. Metereology **8**, 955

Greisen K. 1965 Proc. 9^{th} Inter. Cosmic Ray Conf., London, **2**, 609

————— 1996 Phys. Rev. Lett. **16**, 748; Zatsepin G. T. and Kuz'Min V. A. 1966 JETP Lett. **4**, 78

Harrison T. R., 1960 *Radiation Pyrometry and its underlying Principles of Radiant Heat Transfer* (New York: John Wiley and Sons)

Idso S. B., 1981 *Water Resources Research*, **17-2**, 295

Kakimoto F., Loh E. C., Nagano M., Okuno H., Teshima M., Ueno S., 1996 Nucl. Instrum. Methods **A372**, 527

Larson, T. C., Bruce, S. S., Parr, A. C. 1998 Spectroradiometric Detector Measurements, NIST Special Publication 250-41, US Dept. of Commerce

Longtin D. R., it et al 1988 *A Wind Dependent Desert Aerosol Model: Radiative Properties*, AFGL-TR-88-0112

Martin G. and Matthews J. A. J. 1999 Auger Note: GAP-99-037, http://www-hep.phys.unm.edu/~johnm/GAP_99_037.ps

Olinto A. V. 2000 astro-ph/0002006

Optec 2000 Model LPV-2 Long Path Visibility Transmissometer, Optec, Inc., 199 Smith Street, Lowell, Michigan, U.S.A.

Paltridge G. J., Platt C. M. R. 1981 *Quart. J. R. Meteorol. Soc.* **107**, 367

Prata A. J. 1996 *Quart. J. R. Meteorol. Soc.* **122**, 1127

Roberts, M. 2000 private communication of on-going HiRes *multiple scattering* simulations

Seinfeld J. H. and Pandis S. N. 1998 Atmospheric Chemistry and Physics: From Air Pollution to Climate Change, John Wiley and Sons, Inc.

Sloan R., Shaw J. H. and Williams D. 1955 *J. Opt. Soc. Am.* **45** 455

Sokolsky, P. 1996 Proc. of Int. Sym. on Extremely High Energy Cosmic Rays: Astrophysics and Future Observatories, Ed. M. Nagano, 253.

Song C., Cao Z., Dawson B. R., Fick B. E., Sokolsky P., Zhang X. 1999 astro-ph/9910195

Starlight 2000 Starlight Xpress HX5 high resolution CCD camera, Starlight Xpress Ltd, Foxley Green Farm, Ascot Road, Holyport, Berkshire, England SL6 3LA

Takeda, M. *et al* 1998 Phys. Rev. Lett. **81**, 1163

Tessier, T. *et al* 1999 Proc. of 26^{th} International Cosmic Ray Conference, **5**, 408

Wilkinson, C. R. 1998 The Application of High Precision Timing in the High Resolution Fly's Eye Cosmic Ray Experiment, Thesis, University of Adelaide

Yoshida, S. *et al* 1995 Astropart. Phys. **3**, 105

Yoshida, S. and Dai, H. Y. 1998 J. Phys. **G24**, 905

Zhang, X. 2000 The Multiple Scattering Effect on the Energy Measurement of UHE Cosmic Rays using Atmospheric Fluorescence Technique, Columbia U. preprint

Appendix 1:

The Auger horizontal extinction length measurement will be made at several wavelengths in and near the wavelength acceptance of the fluorescence detectors. Mercury vapor lamps have been chosen for the light source as they have strong emission lines at 365nm, 405nm, 436nm, 546nm and 577nm. The light source includes an intensity monitor to record possible variations in the light intensity with time. The source will also include an optical beam *shutter*. Intensity measurements will be taken with the shutter open and then closed. The difference of these measurements subtracts out any background light in the shutter-open measurements.

The photometer combines an f/2 mirror light collector, interference filters to select the wavelength for each measurement, and a UV sensitive CCD camera (Starlight 2000). The 2-dimensional CCD image provides both good signal isolation as well as a monitor of multiple scattered light.

As noted in Sect 2.1.1, the combined aerosol/Mie and molecular/Rayleigh horizontal extinction length can be obtained using the ratios:

$$\Lambda(\lambda) \;=\; \frac{(r_{far} - r_{near})}{ln(\;\frac{S^{obs}_{near}(\lambda)}{S^{obs}_{far}(\lambda)}\;\cdot\;(\frac{r_{near}}{r_{far}})^2\;)}$$

The fractional measurement uncertainty is given by:

$$\frac{\delta\Lambda(\lambda)}{\Lambda(\lambda)} \;\approx\; \frac{\Lambda(\lambda)}{(r_{far} - r_{near})}\;\{\;\frac{\delta S^{obs}_{near}(\lambda)}{S^{obs}_{near}(\lambda)}\;\oplus\;\frac{\delta S^{obs}_{far}(\lambda)}{S^{obs}_{far}(\lambda)}\;\}$$

where $\oplus$ implies added in quadrature. As the separation of the *near* and *far* lights is $\sim$ 50km, thus $r_{far} - r_{near} \sim 5\Lambda$. As a consequence even $\sim 10\%$ fractional uncertainty in the intensity measurements results in a measurement of the extinction length at the few percent level.

Appendix 2:

The intensity at the LIDAR source/receiver of light backscattered from a height, z, above the LIDAR is given by:

$$I(z,\alpha) \;=\; I_0 \cdot T_{out} \cdot T_{back} \cdot \Big(\frac{1}{\Lambda^m(z)}\Big[\frac{1}{\sigma^m}\Big(\frac{d\sigma^m}{d\Omega}\Big)\Big] \;+\; \frac{1}{\Lambda^a(z)}\Big[\frac{1}{\sigma^a}\Big(\frac{d\sigma^a}{d\Omega}\Big)\Big] \Big)_{180^\circ} \cdot \Delta s \cdot \Delta\Omega$$

where I_0 is the out-going LIDAR beam intensity, α is the viewing angle of the LIDAR to the horizontal, $z/sin(\alpha)$ is the distance from the LIDAR to the point of back-scattering, T_{out} and T_{back} are the transmission factors for the (out-going) light beam and for the scattered (back-coming) light respectively, $\Lambda(z)$ are the light attenuation lengths *per unit distance*, $\Delta s \;=\; c\Delta t/2$, the length of the scattering region is set by the LIDAR time bins, $\Delta\Omega$ is the solid angle subtended by the LIDAR mirror, and $\frac{1}{\sigma}(\frac{d\sigma}{d\Omega})$ are the normalized Rayleigh (superscript "m") and Mie (superscript "a") *phase functions* evaluated for backward scattering.

In the absence of $H.O.$ corrections (which are minimized using narrow field of view LIDAR receivers), the transmission for the out-going light, T_{out}, and the back-coming light, T_{back}, are equal:

$$T_{out} \;=\; T_{back} \;=\; \big(e^{-\tau^m(z)} \cdot e^{-\tau^a(z)}\big)^{1/sin(\alpha)}$$

where the optical depth, $\tau(z)$, is defined in Sect. 2.

In the ratio of backscattered LIDAR measurements from the same altitude, z, but at different angles, α_1 and α_2, several terms cancel including the (potentially unknown) phase functions and attenuation lengths. As the solid angle factors are proportional to the point of light back scattering distance from the LIDAR receiver, $\Delta\Omega \;\propto\; (sin(\alpha)/z)^2$, the ratio becomes:

$$\frac{I(z,\alpha_1)}{I(z,\alpha_2)} \;=\; \big(e^{-\tau^m(z)} \cdot e^{-\tau^a(z)}\big)^{(2/sin(\alpha_1)-2/sin(\alpha_2))} \;\cdot\; \Big(\frac{sin(\alpha_1)}{sin(\alpha_2)}\Big)^2$$

Thus the sum of Rayleigh (molecular) and Mie (aerosol) optical depths are:

$$\tau^m(z) \;+\; \tau^a(z) \;=\; \frac{ln\big[\,\big(\frac{sin(\alpha_2)}{sin(\alpha_1)}\big)^2 \cdot \frac{I(z,\alpha_1))}{I(z,\alpha_2)}\,\big]}{2 \cdot \big(\frac{1}{sin(\alpha_2)} \;-\; \frac{1}{sin(\alpha_1)}\big)}$$

and the uncertainty in the sum is:

$$\delta(\tau^m(z) \;+\; \tau^a(z)) \;\approx\; \frac{1}{2 \cdot \big(\frac{1}{sin(\alpha_2)} \;-\; \frac{1}{sin(\alpha_1)}\big)} \cdot \Big\{ \frac{\delta I(z,\alpha_1)}{I(z,\alpha_1)} \;\oplus\; \frac{\delta I(z,\alpha_2)}{I(z,\alpha_2)} \Big\}$$

where we assume that the fractional uncertainties in the intensities, $I(z,\alpha)$, dominate the error estimate and $\oplus$ implies added in quadrature. As the molecular optical depth, $\tau^m(z)$, will be well determined in Auger (Martin and Matthews 1999) the above relation provides the aerosol optical depth, $\tau^a(z)$, without recourse to an assumed form for the vertical aerosol profile. Furthermore in the 1-dimensional model (for both the molecular atmosphere and for the aerosols) the optical depth, $\tau^a(z)$, is what is needed to make the transmission correction; see Sect. 2.

If the aerosol horizontal extinction length, $\Lambda^a(\lambda)$, is independently measured, see Sect. 2.1.1 and Appendix 1, then the measurement of $\tau^a(z,\lambda) = \int_0^z \frac{\tilde{\rho}(z)dz}{\Lambda^a(\lambda)}$ can be converted into the *effective* aerosol height), h_{eff}:

$$h_{eff}(z) \equiv \Lambda^a(\lambda) \cdot \tau^a(z,\lambda) = \Lambda^a(\lambda) \cdot \int_0^z \frac{\tilde{\rho}(z)dz}{\Lambda^a(\lambda)}$$

which is the integral to height, z, of the aerosol vertical profile (see Sect. 2.2). For $z \sim 0$ then $h_{eff}(z) = z$. In those cases where the normalized aerosol density has a simple exponential dependence on height, $\tilde{\rho}^a(z) = e^{-z/h_a}$, then $h_{eff}(z) = h_a$ once $z >> h_a$. However $h_{eff}(z)$ is more general than these specific cases and allows a straight forward night-to-night comparison of the vertical distribution of the aerosols.